



TITLE:

Encephalomyocarditis virus  
disrupts stress granules, the critical  
platform for triggering antiviral  
innate immune responses.

AUTHOR(S):

Ng, Chen Seng; Jogi, Michihiko; Yoo, Ji-Seung;  
Onomoto, Koji; Koike, Satoshi; Iwasaki, Takuya;  
Yoneyama, Mitsutoshi; Kato, Hiroki; Fujita, Takashi

---

CITATION:

Ng, Chen Seng ...[et al]. Encephalomyocarditis virus disrupts stress granules, the critical platform for triggering antiviral innate immune responses.. Journal of virology 2013, 87(17): 9511-9522

ISSUE DATE:

2013-09

URL:

<http://hdl.handle.net/2433/178797>

RIGHT:

© 2013, American Society for Microbiology.; この論文は出版社版であり  
ません。引用の際には出版社版をご確認ご利用ください。; This is not  
the published version. Please cite only the published version.

EMCV Disrupts Stress Granules, the Critical Platform for Triggering Antiviral Innate Immune Responses

Chen Seng Ng<sup>1,2</sup>, Michihiko Jogi<sup>1,2,3</sup>, Ji-Seung Yoo<sup>1,2</sup>, Koji Onomoto<sup>1,2,3</sup>, Satoshi Koike<sup>4</sup>, Takuya Iwasaki<sup>4</sup>, Mitsutoshi Yoneyama<sup>1,2,3</sup>, Hiroki Kato<sup>1,2</sup>, Takashi Fujita<sup>1,2\*</sup>

<sup>1</sup>Laboratory of Molecular Genetics, Institute for Virus Research, Kyoto University, Kyoto 606-8507, Japan.

<sup>2</sup>Laboratory of Molecular Cell Biology, Graduate School of Biostudies, Kyoto University, Kyoto 606-8507, Japan.

<sup>3</sup>Division of Molecular Immunology, Medical Mycology Research Center, Chiba University, Chiba 260-8673, Japan

<sup>4</sup>Neurovirology Project, Tokyo Metropolitan Institute of Medical Science, Tokyo 156-8506, Japan

**\*Corresponding author. Mailing address:**

Takashi Fujita  
Laboratory of Molecular Genetics,  
Institute for Virus Research,  
Kyoto University,  
Kyoto 606-8507,  
JAPAN.

Phone and Fax: (+81)-75-751-4031  
E-mail: [tfujita@virus.kyoto-u.ac.jp](mailto:tfujita@virus.kyoto-u.ac.jp)

Running title: Loss of stress granule impaired interferon signals.

**Abstract word count:** 244 words

**Text word count:** 4,198 words

**ABSTRACT**

In response to stress, cells induce ribonucleoprotein aggregates, termed stress granules (SGs). SGs are transient loci containing translation-stalled mRNA, which is eventually degraded or recycled for translation. Infection of some viruses including influenza A virus with a deletion of non-structural protein 1 (IAVΔNS1) induces SG-like protein aggregates. Previously, we showed that IAVΔNS1-induced SGs are required for efficient induction of type I interferon (IFN). Here, we investigated SG formation by different viruses using GFP-tagged Ras-GAP SH3 domain binding protein-1 (GFP-G3BP1) as an SG probe. HeLa cells stably expressing GFP-G3BP1 were infected with different viruses and GFP fluorescence was monitored live with time-lapse microscopy. SG formation by different viruses was classified into 4 different patterns: no SG formation, stable SG formation, transient SG formation and alternate SG formation. We focused on EMCV infection, which exhibited transient SG formation. We found that EMCV disrupts SGs by cleavage of G3BP1 at late stages of infection (>8 h) through a similar mechanism to that by poliovirus. Expression of a G3BP1 mutant, which is resistant to the cleavage, conferred persistent formation of SG as well as an enhanced induction of IFN and other cytokines at late stages of infection. Additionally, knockdown of endogenous G3BP1 blocked SG formation with attenuated induction of IFN and potentiated viral replication. Taken together, our findings suggest a critical role of SG as an antiviral platform and shed light on one of the mechanisms by which a virus interferes with host stress and subsequent antiviral responses.

**Keywords:** Encephalomyocarditis virus, melanoma differentiation-associated protein 5, stress-granules, G3BP1, interferon

## INTRODUCTION

In eukaryotic cells, viral infections induce several responses. Cellular pathogen recognition receptors such as RIG-I-like receptors (RLRs), and Toll-like-receptors recognize specific pathogen-associated molecular patterns and activate the transcription of hundreds of genes including interferons (IFNs), inflammatory cytokines and antiviral proteins. Secreted IFNs, in turn, activate a secondary JAK-STAT signaling cascade, which culminate in the activation of various interferon stimulated genes (ISGs) (1,2). A representative ISG, protein kinase RNA-activated (PKR), acts as an antiviral protein by inducing the blockade of viral translation (3-5). PKR is also known to associate with cellular stress-responses. Virus infection results in the accumulation of double-stranded RNA (dsRNA), thereby activating PKR and phosphorylation of eukaryotic initiation factor 2 $\alpha$  (eIF2 $\alpha$ ), leading to the formation of stress granules (SGs) (6,7). Several studies have reported about the interaction between viruses and SGs, especially the effects of specific type of viruses on the fate of SG formation and how viruses modulate stress granule assembly (8-11). Recently, we reported that RLR recruitment to SGs during SG formation is critical in RLR-mediated signaling and non-structural protein 1 of influenza A virus blocks RLR signaling by inhibiting SG and antiviral response (12). Accumulating evidence suggests that viruses have evolved strategies to prevent SG formation. These results suggest that virus-induced SGs potentially serve as platforms for antiviral activity, however, the underlying molecular mechanism still remains to be elucidated.

In the present study, we aim to delineate the physiological impact of stress granule formation and its viral modulation. We employed an EGFP-tagged stress granule marker, Ras-Gap-SH3 domain binding protein (G3BP1) to probe the subcellular distribution of virus-induced SGs (13,14). This system allows us to monitor SGs in an individual virus-infected cell. Infection with RNA and DNA viruses displayed three distinct patterns:



88 stable, transient and alternate formation of SG. We focused on encephalomyocarditis virus  
89 (EMCV), which exhibited transient formation of SGs. We show that EMCV disrupts SGs  
90 through G3BP1 cleavage. Furthermore, we found that EMCV-induced SGs are required for  
91 efficient activation of IFN and cytokine genes. We propose a new antiviral concept  
92 highlighting the potential cross-talk of virus-induced stress responses and activation of the  
93 IFN signaling cascade. This may provide a new insight in understanding the mechanism by  
94 which antiviral genes are regulated.

95  
96

## MATERIALS AND METHODS

**Plasmid constructs.** The stress granule marker constructs pEGFP-C1-G3BP1 (NM\_005754) was a kind gift from Dr. Jamal Tazi (Institute de Génétique Moléculaire de Montpellier, France). pEGFP-C1-G3BP1 Q325E mutant construct was generated by site-directed mutagenesis through KOD-Plus-Mutagenesis kit (TOYOBO, Japan), using primers containing the desired mutation according to manufacturer's instructions, and were completely sequenced by using ABI Prism DNA sequencer to verify the presence of mutation. This plasmid contained a single point amino acid substitution at position 325 (from glutamine to glutamate), which is resistant to cleavage by 3C<sup>PRO</sup> of Poliovirus (PolioV) (15). Expression vectors for EMCV pF-leader and pF-3C protease were described previously (16).

**Viruses.** PolioV (Mahoney strain), vesicular stomatitis virus (VSV, Indiana strain), EMCV, adenoviruses (Type5), Sindbis virus (SINV) and Theiler's murine encephalomyelitis virus (TMEV, GDVII strain) were prepared by infecting BHK cells at a multiplicity of infection (MOI) of 1. Cell culture medium was collected after confirming cytopathic effects following infection. Medium containing newly produced viruses was centrifuged at 1,500rpm for 5 min to pellet down the cell debris, supernatant containing viruses were collected and stored at -80°C. Viral titer was assessed by plaque assay on L929 cells as previously described (17). NDV (Miyadera strain), Sendai virus (Cantell, SeV) and influenza A virus with a deletion of the NS1 gene (IAVΔNS1, strain A/Puerto Rico 8/34) (18,19) were propagated in the allantoic cavities of embryonated chicken eggs, then stocks were stored at -80°C.

**Generation of stable HeLa cells and general cell culture conditions.** Cell lines were maintained in Dulbecco's Modified Eagle's medium (DMEM) supplemented with 10%

heat-inactivated fetal bovine serum (Nacalai Tesque, Japan) and Penicillin-Streptomycin (100U/mL and 100μg/mL respectively, Nacalai Tesque, Japan). To generate HeLa cells stably expressing EGFP-G3BP1 wild type and Q325E mutant, pEGFP-C1-G3BP1 and pEGFP-C1-G3BP1 Q325E mutant expression constructs was linearized by restriction enzyme ApaL1 (Takara, Japan). The linearized plasmids were then transfected into HeLa cells using FuGENE6 (Promega, USA) according to manufacturer's recommendations. Transformants were selected by including 1 mg/mL of G418 in the culture medium. Individual colonies were isolated and characterized.

**Live-cell imaging and immunofluorescence microscopy.** For the live-cell imaging analysis, HeLa cells stably expressing EGFP-G3BP1 (HeLa/G-G3BP) were seeded in 12-well plate and incubated at 37°C. After 24 hours, cells were washed with DMEM medium (10% fetal bovine serum and 1% Penicillin-Streptomycin) for several rounds. Cells were then infected with various types of RNA and DNA viruses. After 1 hour infection, virus was removed and replaced with 1.0 mL of DMEM imaging medium (4,500 mg/L D-glucose and L-glutamine, 25mM HEPES buffer, no sodium pyruvate and phenol red, Invitrogen). Imaging was immediately initiated every 10mins. Live cells were maintained on the microscope stage at 37°C, with 5% carbon-dioxide in a humidity-controlled chamber. Images were mounted using Biophotonics-ImageJ software. All imaging was performed by using a Leica CTR 6500.

For the immunofluorescence analysis, cells were seeded either in a 12-well plate or a 8-well chamber slide and incubated at 37°C. After 24 hours, cells were subjected to various treatments such as plasmid transfection or virus infection. Cells were then rinsed in phosphate-buffered saline (PBS) several times, fixed with 4% paraformaldehyde solution for 10 min at room temperature, washed with PBS for two additional rounds, permeabilized with

acetone:methanol (1:1) for one minute, and blocked with phosphate-buffered saline containing 0.1 % Tween-20 (PBST) solution containing bovine serum albumin (BSA, 5.0 mg/mL) for 1 hour at 4°C. Cells were then incubated with primary antibody, followed by fluorophores-conjugated secondary antibodies (Invitrogen) for one-hour at 4°C. Cells were washed with PBST extensively and mounted. All images were obtained by a Leica CTR 6500.

**siRNA-directed gene silencing.** The siRNA universal negative control and siRNA targeting stress granule marker-G3BP1 (50nM) and dsRNA protein kinase PKR were purchased from Invitrogen, and transfected using either Lipofectamine2000 (Invitrogen) or RNAiMax (Invitrogen) according to manufacturer's recommendation. The sequence of siRNA: RIG-I, sense 5'-CGG AUU AGC GAC AAA UUU AUU-3', antisense 5'-UAA AUU UGU CGC UAA UCC GUU-3'; PKR#1, sense 5'-UUU ACU UCA CGC UCC GCC UUC UCG U-3', antisense 5'-ACG AGA AGG CGG AGCGUGAAGUAA A -3'; PKR#2, sense 5'- AUG UCA GGA AGG UCA AAU CUG GGU G-3', antisense 5'-CAC CCA GAU UUG ACC UUC CUG ACA U-3'; G3BP1, sense 5'-UAA UUU CCC ACC ACU GUU AAU GCG C-3', antisense 5'-GCGCAUUAACAGUGGUGGGAAAUUA-3'. After 48 hours post-transfection, cells were subjected to viral infection or other treatments. A specific antibody for G3BP1 (Santa Cruz) was used to monitor the knockdown efficiency.

**RNA analysis.** RNA was harvested from cells with TRIzol (Invitrogen) according to the manufacturer's instructions. Contaminating DNA was then eliminated by using recombinant DNase I (Roche, 10 units/μL) according to the manufacturer's protocol. Treated samples were purified by phenol-chloroform extraction. 500 ng of purified RNA was used as a template to synthesize cDNA using a High Capacity cDNA Reverse-Transcription kit

173 (Applied Biosystem) as specified by the manufacturer through the following cycles: 25°C for  
174 10 seconds; 37°C for 2 hours; 85°C for 10 seconds. The concentration of cDNA was  
175 quantified by a spectrophotometer and the final concentration was adjusted to 1 µg/µL.  
176 cDNA samples were then either subjected to standard PCR or real-time quantitative-PCR  
177 analysis with specific probes from Taqman Gene Expression Assay (Applied Biosystem).  
178 Quantification of EMCV viral RNA was performed using SYBR master mix (Applied  
179 Biosystem) with specific primers targeting EMCV capsid coding region. Standard PCR was  
180 performed with cDNA samples together with a master mix containing 1X PCR buffer,  
181 2.5mM of each dNTP's, 0.2 units of ExTaq Polymerase and 1.0µM of both forward and  
182 reverse primers. PCR buffer, dNTPs and ExTaq Polymerases were purchased from Takara,  
183 Japan. Primers were all customized and purchased from Invitrogen. PCR was performed in  
184 50 µL reaction mixture with initial annealing temperature at 56°C-60°C. PCR products were  
185 analyzed by agarose gel electrophoresis.

186

187 **Western blotting.** Cells were collected in ice-cold PBS by scraper. Cells were collected  
188 by centrifugation and lysed by NP-40 buffer (50mM Tris [pH8.0], 150mM NaCl, 1%  
189 [vol/vol] NP-40, 1 nM of Vanadate, 1 mM of Leupeptin and phenylmethanesulfonylfluoride),  
190 followed by centrifugation at 15,000rpm for 10 min and ultracentrifugation at 100,000rpm for  
191 5min. The supernatant was mixed with an equal volume of 2X SDS buffer, boiled for 5 min,  
192 separated by SDS-PAGE (30µg/lane), and transferred to nitrocellulose membrane. The  
193 membranes were incubated in blocking buffer (PBS, 5% [wt/vol] dry milk powder) for 30min  
194 at room temperature, followed by incubation with primary antibody diluted in blocking buffer  
195 at 4°C overnight. Membranes were washed extensively with TBST (TBS, 0.1% Tween-20),  
196 followed by incubation with a conjugated-secondary antibody for 1 hour at room temperature.  
197 The proteins were visualized using alkaline-phosphatase buffer containing BCIP-NBT

198 (Promega) color development substrate (100 mM Tris-HCl [pH9.0], 150 mM NaCl, 1 mM  
199  $MgCl_2$ , 66  $\mu$ L of NBT [50 mg/mL] and 33  $\mu$ L of BCIP [50mg/mL]).

200

201 **Antibodies.** The antibodies used in this study include mouse monoclonal anti-GFP (1:1000,  
202 MBL); goat polyclonal anti-G3BP1 (1:500, Santa Cruz sc-70283); mouse monoclonal  
203 anti-G3BP1 (1:1000, Santa Cruz sc-365338); rabbit polyclonal anti-PKR (1:1000, Santa Cruz  
204 sc-709); rabbit polyclonal anti-TIA1/R (1:1000, Santa Cruz sc-48371); goat polyclonal  
205 anti-TIAR (1:1000, Santa Cruz sc-1749); rabbit polyclonal anti-HuR (1:1000, Santa Cruz  
206 sc-365816); Propidium iodide [PI] (1:2000 in PBST, Miltenyi Biotec). The RIG-I antibody  
207 were generated by immunizing a rabbit with a synthetic peptide corresponding to amino acid  
208 793-807 of RIG-I and MDA5. Mouse monoclonal anti-PABP (1:1000, Abcam ab6125);  
209 rabbit monoclonal anti-actin (1:5000; BioLegend Poly6221); mouse anti-FLAG (1:1000,  
210 Sigma Aldrich) and rabbit monoclonal anti-phospho-PKR pT446 (1:1000, Epitomics Inc.).  
211 Anti-EMCV polyclonal antibody was obtained by immunizing a rabbit with purified EMCV  
212 virions. Anti-MDA5 polyclonal antibody was obtained by immunizing a rat with recombinant  
213 MDA5 (produced in insect cells) which was pre-activated with RNA ligands.

214

215 **Quantification for the distribution pattern of virus-induced SG.** SG formation was  
216 quantified visually by using eye-sight counting. The total number of cells displaying each  
217 unique distribution pattern in each location was recorded and the percentage for each pattern  
218 was calculated. As for the fixed cells, 10 pictures at different locations were taken randomly.  
219 Cells displaying SG foci were quantified manually. Graphs display the average percentage of  
220 replicates (at least 20 times).

221

222

223

## RESULTS

**Characterization of HeLa cells stably expressing SG marker, G3BP1.** To monitor SGs in living cells, we generated HeLa/G-G3BP (Fig. 1). Constitutive aggregation of intrinsic SG components is reported to lead to a severe stall in protein synthesis and eventual apoptosis (14,20). All the HeLa/G-G3BP clones displayed uniform and high GFP expression and their growth rate was comparable to the parental cells (our unpublished observation). It has been well documented that G3BP1 accumulates in SG foci in response to arsenite treatment (oxidative stress) and virus infection (12,13). HeLa/G-G3BP clone 12 was treated with arsenite or infected with Newcastle disease virus (NDV) or Influenza A virus (IAV) with an NS1 deletion (IAV $\Delta$ NS1), then the GFP localization was examined by confocal microscopy. As shown in Fig. 1A, speckle-like localization of GFP was induced by these stimuli. Other clones also exhibited similar speckle formation after arsenite treatment or NDV infection (Fig. 1B, C). We confirmed that other SG components, TIA-1, TIAR, HuR and eIF3 colocalized with the GFP speckles (unpublished observation). These results indicate that EGFP-G3BP1 acts as a suitable probe for virus-induced SGs. However, since transient overexpression of G3BP1 results in SG formation without external stress (13), we tested if the HeLa/G-G3BP clones would exhibit normal antiviral response. As shown in Fig. 1D, all clones exhibited comparable induction of IFN- $\beta$  mRNA as parental cells. We chose clone 18 for further analyses.

**G3BP1 exhibits three redistribution patterns after infection with both RNA and DNA viruses.** To examine the dynamics of cytoplasmic SGs induced by viral infection, the cells were infected with different viruses as shown in Fig. 2 and monitored live for distribution of GFP fluorescence (representative results are shown in Movie S1-S9). Cells infected with SeV, IAV, VSV and TMEV did not show SG formation (8). Other viruses induced SGs, typically

forming a large number of small granules around 5 h post infection and gradually fusing to each other. SG formation was quantified (Fig. 2A-K) and classified into three predominant patterns: stable formation (Fig. 2L), transient formation (Fig. 2M), and alternating formation (Fig. 2N) within a single cell. NDV, IAVΔNS1 and Adenovirus 5 displayed a stable formation of SGs (Movie S1-S3). Whereas SINV, EMCV and PolioV induced foci at around 5 to 6 h post infection, however, the foci disappeared thereafter (transient formation) (Fig. 2D-2F; Movie S4-S6). Interestingly, adenovirus 5 with E1A deletion, exhibited multiple rounds of formation and disappearance of SGs (alternate formation) in the majority of cells (Fig. 2I; Movie S7). Similar oscillation of SGs in cells infected with HCV and treated with IFN was reported (21). Collectively, these live-cell imaging analyses demonstrated that viral infections trigger host stress responses, however different viruses induce distinct response patterns, presumably through specific underlying mechanisms. The observed SG formation patterns are unlikely due to G3BP1 overexpression because wt HeLa cells exhibited transient SG formation upon EMCV infection when endogenous G3BP1 was used as a marker (Fig. 2O).

**EMCV infection results in the cleavage of G3BP1.** We focused on the mechanism of transient formation of SGs by EMCV because PolioV has been reported to inhibit SG formation by cleavage of G3BP1 (15). We examined if EGFP-G3BP1 is cleaved by EMCV by Western blotting. EGFP-G3BP1 fusion protein is detected as a polypeptide of 96 kDa and EMCV infection resulted in the appearance of an 80 kDa GFP-containing protein at 6 h post infection and nearly complete cleavage of EGFP-G3BP1 reached near completion at 10 h post infection (Fig. 3A). Because the fusion protein contains an EGFP moiety at the N-terminus of G3BP, the cleavage of G3BP1 is likely to occur at the C-terminal region of G3BP1. We verified the cleavage site by using an antibody detecting the C-terminal epitope



of G3BP1 (Fig. S1A and B). Because the mapped cleavage site was close to that by PolioV and the cleavage by PolioV is prevented by amino acid substitution within G3BP1 (Q325E) (15), we therefore examined this mutant for cleavage by EMCV (Fig. 3B). We found that G3BP1 Q325E was resistant to cleavage by EMCV, suggesting a common cleavage mechanism. To examine whether the disruption of SG by EMCV is solely due to cleavage of G3BP1, we examined other SG components, PABP, TIA-1/R, HuR and PKR, which are also essential for SG formation. Fig. 3C shows that the levels of SG components with the exception of G3BP1 did not change upon EMCV infection and that G3BP1 cleavage coincided with the detection of EMCV proteins. Expression of EMCV 3C protease but not leader protein by transfection was sufficient to reproduce G3BP1 cleavage at Q325 (Fig. 3D), strongly suggesting that the cleavage is mediated by 3C protease. We next examined SG formation of HeLa/G-G3BPQ325E. In sharp contrast to the cells expressing wild type G3BP1 (Movie S6), HeLa/G-G3BPQ325E exhibited stable formation of SGs as judged by single cell imaging (Fig. 4A and B; Movie S8) and quantification (Fig. 4C). These results suggest that EMCV disrupts SGs by cleavage of G3BP1 through a similar mechanism as PolioV.

**G3BP1 negatively regulates EMCV replication.** To examine the impact of SG disruption on EMCV replication, we infected both HeLa/G-G3BP and HeLa/G-G3BPQ325E with EMCV and analyzed viral replication by RT-qPCR (Fig. 5A). EMCV RNA recovered from HeLa/G-G3BP was six fold higher compared with that of HeLa/G-G3BPQ325E. Similarly, a significantly lower viral yield was observed with cells expressing G3BP1 Q325E, suggesting that SG formation is critical for suppressing EMCV replication. To further confirm the involvement of G3BP1, we depleted endogenous G3BP1 by siRNA-mediated knockdown (Fig. 5B) and examined its effect on EMCV replication. G3BP1 knockdown caused increased

EMCV replication as judged by the approximate 5-fold augmentation of viral RNA and viral yield (Fig. 5B). These results suggest that G3BP1 is involved in the negative regulation of EMCV.

**G3BP1 is critical for EMCV-induced interferon and cytokine gene activation.** Based on the above findings, we next asked how G3BP1 exerts its antiviral role. The type I interferon system constitutes major innate antiviral responses, therefore we examined EMCV-induced IFN- $\beta$  gene activation in HeLa/G-G3BP and HeLa/G-G3BPQ325E (Fig. 6). In HeLa/G-G3BP cells, IFN- $\beta$  mRNA accumulated at 4 h post infection, followed by a gradual decrease. However, IFN- $\beta$  mRNA levels persisted in HeLa/G-G3BPQ325E after 8 h post infection (Fig. 6B). In agreement with these results, the amount of IFN- $\beta$  protein released into the culture medium at 24 h is significantly augmented by Q325E mutation (Fig. 6A). Similar enhancement of cytokine mRNA was observed for CXCL10, IL-6 and RANTES (Fig. 6C-E). We investigated gene activation at early time points between 0 to 4 h, and observed similar activation kinetics between HeLa/G-G3BP and HeLa/G-G3BPQ325E (Fig. 7), suggesting that the reduced gene activation of HeLa/G-G3BP is due to G3BP1 cleavage. Q325E mutation did not affect the IFN- $\beta$  gene induction in the case of IAV $\Delta$ NS1, which did not cause G3BP1 cleavage (Fig. 6F). Next, we examined the effects of depleting endogenous G3BP1 on cytokine gene activation. As expected, knockdown of endogenous G3BP1 attenuated IFN- $\beta$  and other cytokine gene expression (Fig. 8A-D). These results strongly suggest that G3BP cleavage leads to attenuation of antiviral cytokine induction.

It has been well documented that MDA5 senses EMCV infection (22-25), and that virus- and oxidative stress-induced SGs recruit RIG-I, MDA5 and LGP2 (12). Therefore, we hypothesized that EMCV-induced SG regulates IFN- $\beta$  gene activation by facilitating MDA5 activation. We examined MDA5 localization in EMCV-infected HeLa cells by

immunostaining. MDA5 displayed re-localization to speckle-like granules upon EMCV infection (Fig. 9A). The speckles also contain endogenous G3BP1 (Fig. 9A) and TIAR (Fig. 9B). Interestingly, PI, a dye that binds to dsDNA and dsRNA, stains cytoplasmic speckles found only in virus-infected cells and the dsRNA speckles are co-localized with G3BP1 and TIAR. These observations suggest that EMCV infection induces SGs, which recruit SG markers, MDA5 and EMCV dsRNA.

331

**PKR is essential for SG-formation and IFN-induction in EMCV infection.** Various types of viruses were shown to induce SG formation through PKR activation (26-28). We therefore examined whether EMCV induces SG formation in a PKR-dependent manner. Endogenous PKR expression was efficiently downregulated by siRNA (Fig. 10A). Under these conditions, SG formation by EMCV was decreased significantly (Fig. 10A). We next asked whether cleavage of G3BP1 results in PKR dephosphorylation. Immunoblot analyses showed that PKR was autophosphorylated at 4 h post infection, however at 12 h, when G3BP1 cleavage was nearly complete, PKR phosphorylation was undetectable (Fig. 10B, Lane 3), suggesting that G3BP1 cleavage resulted in PKR dephosphorylation. Finally, we examined whether the final outcome of the signaling, IFN- $\beta$  gene expression, was dependent on PKR. In PKR knockdown cells, the induction of IFN- $\beta$  mRNA by EMCV was significantly decreased compared to control cells (Fig. 10C). We further confirmed previous reports that IFN induction by PolyI:C or IAV $\Delta$ NS1 infection was PKR dependent (12). From the data presented above, we concluded that loss of PKR impaired EMCV-induced SG formation, leading to a reduction of IFN- $\beta$  gene activation.

347

## DISCUSSION

Viral infection causes stress in host cells, resulting in SG formation. To date, both pro- and anti-viral roles have been described for virus-induced SGs (28-30) and this issue remains controversial.

In this study, we demonstrated that SGs are potentially involved in mediating virus-triggered IFN responses. It was reported that PolioV 3C protease cleaves G3BP1 at the residue of Q325, resulting in the disruption of SGs (15). The observation indicates that G3BP1 is not only a component of SGs but also its inactivation by cleavage causes the disruption of SGs. Here, we show that EMCV shares G3BP cleavage activity with identical specificity to PolioV 3C requiring intact Q325. Interestingly, Coxsackie virus also disrupts SG (31) by a similar mechanism (Fung et al unpublished observation), suggesting that this strategy is shared by some picornaviruses to evade immune responses. At the early phase of EMCV infection, cleavage of G3BP1 was not evident. However, at 4 hpi, cleavage was detectable, and at 10 h, cleavage reached completion, suggesting that the accumulation of 3C is necessary for the disruption. We observed that stable expression of G3BP1 Q325E blocked the disassembly of SGs as well as enhanced IFN- $\beta$  production at a late phase of infection. Furthermore, knockdown experiments showed that G3BP1 is necessary for efficient activation of the IFN- $\beta$  gene, particularly at the later stages of infection. Although it was reported that PolioV 3C cleaves RIG-I and MDA5 (32), and EMCV cleaves RIG-I (33), we did not observe these cleavages even under the conditions in which G3BP1 was cleaved by EMCV or PolioV (Fig. 11). Taken together, we conclude that G3BP1 is a physiological regulator of IFN- $\beta$  gene induction through the formation of SGs, which recruits the RNA sensor MDA5. In addition, the persistent activation of the IFN- $\beta$  gene at late time points is likely due to the increase of the local concentration of both MDA5 and its ligands within the condensed granules.

Collectively, the data presented above strongly suggest that 3C protease of EMCV acts as critical factor for evading host IFN production to ensure efficient replication. It was demonstrated that PKR plays a critical role in dsRNA- or IAV $\Delta$ NS1-induced SG formation and subsequent IFN- $\beta$  gene activation (12). Our observation that PKR is required for efficient IFN gene activation by EMCV, suggests that PKR is responsible for initiating the SG formation (Fig. 10).

Considering that the assembly of SGs is a part of antiviral response of the host, it is plausible that viruses evolve strategies to block it. Indeed, IAV, SeV and TMEV do not induce SG (Fig. 2) and it was reported that leader RNA, NS1 and leader protein are responsible for the inhibition, respectively (8,12,34). Although TMEV belongs to *Picornaviridae*, their mechanism of SG inhibition appeared to be distinct from those of EMCV and PolioV. TMEV and Mengovirus inhibit SG by the action of leader protein (8,31). We found that 3C but not the leader protein of EMCV inhibits SG formation (Fig. 12). It is tempting to speculate that leader of TMEV and Mengovirus inhibit IFN production (35,36) through the blockade of SG formation, where RLR and viral RNA efficiently interact, as one of the mechanisms. Interestingly, although the leader of EMCV did not affect SGs, it inhibits IFN gene activation (Fig. 12), suggesting that leaders of different cardioviruses are functionally equivalent (37,38), however through distinct mode of action. Therefore, these viruses encode multiple inhibitory proteins to efficiently manipulate host immune responses. EMCV and SINV induced SG at early time points after infection but the SG formation was disrupted later. A similar phenomenon was reported for West Nile and Dengue viruses by monitoring TIA-1/R as a SG marker (29). In the case of EMCV and PolioV, G3BP1 cleavage by viral 3C protease is responsible for the disassembly of the SG. Therefore, active mechanisms for the disruption of SGs by SINV, West Nile and Dengue viruses have been suggested, although underlying mechanisms remain to be determined. In addition to transient

formation of SGs, some viruses exhibited alternating formation of SGs; SGs were formed at an early stage then disappeared and re-formed at a later stage. This alternating pattern is also dependent on the cell lines used (unpublished observation), suggesting that the pattern of SG formation is determined by a dynamic balance between host antiviral response and viral inhibitory mechanism (21). Such a host mechanism could be a therapeutic target to enhance host defense against viruses.

Here we provide evidence that EMCV-induced SGs are involved in regulating IFN- $\beta$  gene expression. Thus, virus-induced SGs might play dual roles: (i) suppressing viral replication through an inhibition of viral protein synthesis, and (ii) serving as a platform to facilitate IFN- $\beta$  production.

## ACKNOWLEDGEMENTS

We thank Dr. Jamal Tazi for providing pEGFP-G3BP1, Dr. A.C. Palmenberg for expression vectors for EMCV leader and 3C proteins, Gabriel Fung (University of British Columbia) and Dr. Peter Gee (Kyoto University) for proofreading the manuscript. This research was supported by the following grants. The Ministry of Education, Culture, Sports, Science and Technology (MEXT) of Japan (Innovative Areas “Infection competency” (No.24115004), Scientific Research “A”(23249023)), the Ministry of Health, Labor and Welfare of Japan, the Uehara Memorial Foundation, the Mochida Memorial Foundation for Medical and Pharmaceutical Research, the Takeda Science Foundation, the Naito Foundation, and Nippon Boehringer Ingelheim. N.C.S. is a recipient of Monbukagakusho fellowship from MEXT. All authors declare no conflict of interest.

421 **REFERENCES**

- 422 1. **Meylan E, Tschopp J and Karin M.** 2006. Intracellular pattern recognition receptors  
423 in the host response. *Nature* **442**:39-44.
- 424 2. **Darnell Jr JE, Kerr IM and Stark GR.** 1994. Jak-STAT pathways and  
425 transcriptional activation in response to IFNs and other extracellular signaling  
426 proteins. *Science* **264**:1415-1421.
- 427 3. **Garcia J MA, Ventoso GI, Guerra S, Domingo E, Rivas C and Esteban M.** 2006.  
428 Impact of Protein Kinase PKR in Cell Biology: from antiviral to antiproliferative  
429 action. *Microbiol. & Mol. Biol. Reviews* **70**:1032-1060.
- 430 4. **Der S. and Lau AS.** 1995. Involvement of the double-stranded-RNA-dependent  
431 kinase PKR in interferon expression and interferon-mediated antiviral activity. *Proc.*  
432 *Natl. Acad. Sci. USA* **92**:8841-8845.
- 433 5. **Terenzi F, DeVeer M, Ying H, Restifo NP, Williams BR and Silverman RH.** 1999.  
434 The antiviral enzymes PKR and RNase L suppress gene expression from viral and  
435 non-viral based vectors. *Nucleic acids Research* **27**:4369-4375.
- 436 6. **McInerney GM, Kedersha NL, Kaufman RJ, Anderson P and Liljeström P.** 2005.  
437 Importance of eIF2 $\alpha$  phosphorylation and stress granule assembly in Alphavirus  
438 Translation Regulation. *Mol. Biol. Cell.* **16**:3753-3763.
- 439 7. **White, JP and Lloyd RE.** 2012. Regulation of stress granules in virus systems.  
440 *Trends Microbiol.* **20**:175-183.
- 441 8. **Borghese F. and Michiels T.** 2011. The leader protein of cardioviruses inhibits stress  
442 granule assembly. *J. Virol.* **85**:9614-9622.
- 443 9. **Katoh H, Okamoto T, Fukuhara T, Kamban H, Morita E, Mori Y, Kamitani W**  
444 **and Matsuura Y.** 2013. Japanese Encephalitis virus core protein inhibits stress

- 445 granule formation through an interaction with Caprin-1 and facilitates viral  
446 propagation. *J. Virol.* **87**:489-502.
- 447 10. **Okonski KM and Samuel CE.** 2013. Stress granule formation induced by measles  
448 virus is protein kinase PKR-dependent and impaired by RNA Adenosine deaminase  
449 ADAR1. *J. Virol.* **87**:756-766.
- 450 11. **Dinh PX, Beura LK, Das PB, Panda D, Das A and Pattnaik AK.** 2013. Induction  
451 of stress granule (SG)-like structures in vesicular stomatitis virus-infected cells. *J.*  
452 *Virol.* **87**:372-383.
- 453 12. **Onomoto K, Jogi M, Yoo JS, Narita R, Morimoto S, Takemura A, Sambhara S,**  
454 **Kawaguchi A, Osari S, Nagata K, Matsumiya T, Namiki H, Yoneyama M and**  
455 **Fujita T.** 2012. Critical role of an antiviral stress granule containing RIG-I and PKR  
456 in viral detection and innate immunity. *PLoS One* **7**:e43031.
- 457 13. **Tourrière H, Chebli K, Zekri L, Courselaud B, Blanchard JM, Bertrand E and**  
458 **Tazi J.** 2003. The RasGAP-associated endoribonuclease G3BP assembles stress  
459 granules. *J. Cell Biol.* **160**:823-831.
- 460 14. **Kedersha N, Tisdale S, Hickman T and Anderson P.** 2008. Real-Time and  
461 quantitative imaging of mammalian stress granules and processing bodies. *Methods in*  
462 *Enzymology* **448**:521-552.
- 463 15. **White JP, Cardenas AM, Marissen WE and Lloyd RE.** 2007. Inhibition of  
464 cytoplasmic mRNA stress granule formation by a viral proteinase. *Cell Host Microbe*  
465 **15**:295-305.
- 466 16. **Porter FW, Bochkov YA, Albee AJ, Wiese C. and Palmenberg AC.** 2006. A  
467 picornavirus protein interacts with Ran-GTPase and disrupts nucleocytoplasmic  
468 transport. *Proc. Natl. Acad. Sci. USA* **103**:12417-12422.



- 469 17. **Ouda R, Onomoto K, Takahasi K, Edwards MR, Kato H, Yoneyama M and**  
470 **Fujita T.** 2011. Retinoic acid-inducible gene I-inducible miR-23b inhibits infections  
471 by minor group rhinoviruses through down-regulation of the very low density  
472 lipoprotein receptor. *J. Biol. Chem.* **286**:26210-26219.
- 473 18. **Garcia-Sastre A, Egorov A, Matassov D, Brandt S, Levy DE, Durbin JE, Palese P**  
474 **and Muster T.** 1998. Influenza A virus lacking the NS1 gene replicates in  
475 interferon-deficient systems. *Virology* **252**:324-330.
- 476 19. **Tisoncik JR, Billharz R, Burmakina S, Belisie SE, Proll SC, Korth MJ,**  
477 **Garcia-Sastre A and Katze MG.** 2011. The NS1 protein influenza A virus suppresses  
478 interferon-regulated activation of antigen-presentation and immune-proteasome  
479 pathways. *J. Gen. Virol.* **92**:2093-2104.
- 480 20. **Kharraz Y, Salmand PA, Camus A, Auriol J, Gueydan C, Kruys V and Morello**  
481 **D.** 2010. Impaired embryonic development in mice overexpressing the RNA-binding  
482 TIAR. *PLoS One* **5**:e11352.
- 483 21. **Ruggieri A, Dazert E, Metz P, Hofmann S, Bergeest JP, Mazur J, Bankhead P,**  
484 **Hiet MS, Kallis S, Alvisi G, Samuel CE, Lohmann V, Kaderali L, Rohr K, Frese**  
485 **M, Stoecklin G and Bartenschlager R.** 2012. Dynamic oscillation of translation and  
486 stress granule formation mark the cellular response to virus infection. *Cell Host*  
487 *Microbe* **12**:71-85.
- 488 22. **Kato H, Sato S, Yoneyama M, Yamamoto M, Uematsu S, Matsui K, Tsujimura T,**  
489 **Takeda K, Fujita T, Takeuchi O and Akira S.** 2005. Cell type-specific involvement  
490 of RIG-I in antiviral response. *Immunity* **23**:19-28.
- 491 23. **Kato H, Takeuchi O, Sato S, Yoneyama M, Yamamoto M, Matsui K, Uematsu S,**  
492 **Jung A, Kawai T, Ishii KJ, Yamaguchi O, Otsu K, Tsujimura T, Koh CS, Reis e**

- 493        **Sousa C, Matsuura Y, Fujita T and Akira S.** 2006. Differential roles of MDA5 and  
494        RIG-I helicases in the recognition of RNA viruses. *Nature* **441**:101-105.
- 495    24.   **Ng CS, Kato H and Fujita T.** 2012. Recognition of viruses in the cytoplasm by  
496        RLRs and other helicases-how conformational changes, mitochondrial dynamics and  
497        Ubiquitination control innate immune responses. *Int. Immunol.* **24**:739-749.
- 498    25.   **Feng Q, Hato SV, Langereis MA, Zoll J, Virgen-Slane R, Peisley A, Hur S,**  
499        **Semler BL, van Rij RP and van Kuppeveld FJ.** 2012. MDA5 detects the  
500        double-stranded RNA replicative form in picornavirus-infected cells. *Cell Rep*  
501        **2**:1187-1196.
- 502    26.   **Lindquist ME, Mainou BA, Dermody TS and Crowe JE Jr.** 2011. Activation of  
503        protein kinase R is required for induction of stress granules by respiratory syncytial  
504        virus but dispensable for viral replication. *Virology* **413**:103-110.
- 505    27.   **Khaperskyy DA, Hatchette TF and McCormick C.** 2012. Influenza A virus inhibits  
506        cytoplasmic stress granule formation. *FASEB J.* **26**:1629-1639.
- 507    28.   **Simpson-Holley M, Kedersha N, Dower K, Rubins KH, Anderson P, Hensley LE**  
508        **and Connor JH.** 2011. Formation of antiviral cytoplasmic granules during  
509        orthopoxvirus infection. *J. Virol.* **85**:1581-1593.
- 510    29.   **Emara MM and Brinton MA.** 2007. Interaction of TIA-1/TIAR with West Nile and  
511        dengue virus products in infected cells interferes with stress granule formation and  
512        processing body. *Proc. Natl. Acad. Sci. USA* **104**:9041-9046.
- 513    30.   **Qin Q, Hastings C and Miller CL.** 2009. Mammalian orthoreovirus particles induce  
514        and are recruited into stress granules at early times postinfection. *J. Virol.*  
515        **83**:11090-11101.

- 516 31. **Langereis MA, Feng Q and van Kuppeveld FJ.** 2013. MDA5 localizes to stress  
517 granules but this localization is not required for the induction of type I interferon. *J.*  
518 *Virol.* (doi: [10.1128/JVI.03213-12](https://doi.org/10.1128/JVI.03213-12)).
- 519 32. **Barral PM, Morrison JM, Drahos J, Gupta P, Sarker D, Fisher PB and**  
520 **Racaniello VR.** 2007. MDA-5 is cleaved in Poliovirus-infected cells. *J. Virol.*  
521 **81:**3677-3684.
- 522 33. **Barral PM, Sarkar D, Fisher PB and Racaniello VR.** 2009. RIG-I is cleaved  
523 during picornavirus infection. *Virology* **391:**171-176.
- 524 34. **Iseni F, Garcin D, Nishio M, Kedersha N, Anderson P and Kolakofsky D.** 2002.  
525 Sendai virus trailer RNA binds TIAR, a cellular protein involved in virus-induced  
526 apoptosis. *The EMBO J* **21:**5141-5150.
- 527 35. **Ricour C, Delhay S, Hato SV, Olenyik TD, Michel B, van Kuppeveld FJ, Gustin**  
528 **KE and Michiels T.** 2009. Inhibition of mRNA export and dimerization of interferon  
529 regulatory factor 3 by Theiler's virus leader protein. *J Gen Virol.* **90:**177-186.
- 530 36. **Delhay S, van Pesch V and Michiels T.** 2004. The leader protein of Theiler's virus  
531 interferes with nucleocytoplasmic trafficking of cellular proteins. *J. Virol.*  
532 **78:**4357-4362.
- 533 37. **Paul S and Michiels T.** 2006. Cardiovirus leader proteins are functionally  
534 interchangeable and have evolved to adapt to virus replication fitness. *J. Gen Virol.*  
535 **87:**1237-1246.
- 536 38. **Hato SV, Ricour C, Schulte BM, Lanke KH, de Bruijini M, Zoll J, Melchers WJ,**  
537 **Michiels T and van Kuppeveld FJ.** 2007. The mengovirus leader protein blocks  
538 interferon-alpha/beta gene transcription and inhibits activation of interferon regulatory  
539 factor 3. *Cell Microbiol.* **9:**2921-2930.

540

## Figure Legends

**FIG 1. Characterization of HeLa/G-G3BP cells.** (A) HeLa/G-G3BP1 clone 12 was mock treated or stimulated as indicated. Cells were fixed and examined for GFP fluorescence. Four independent HeLa/G-G3BP cell clones were stimulated by arsenite (B) or by infection with NDV (C) and % of GFP speckle positive cells was determined. (D) Parental HeLa cells and HeLa/G-G3BP1 clones were infected with NDV for 12 h and IFN - $\beta$  gene expression was determined by RT-qPCR. (Error bars,  $\pm$ S.D. of duplicates, N=2).

**FIG 2. Three major forms of virus-induced stress granule distribution pattern in HeLa/G-G3BP cells infected with different viruses.** HeLa/G-G3BP cells were infected with (A) NDV, (B) IAV, (C) IAV $\square$ NS1, (D) EMCV, (E) SINV, (F) PolioV, (G) SeV, (H) VSV, (I) adenovirus 5 with E1A deletion (Adeno5 $\square$ E1A), (J) adenovirus 5 wild type (Adeno5WT) and (K) TMEV for 9~12 h and SG formation was monitored and quantified as described in materials and methods. (Error bars,  $\pm$ S.D. of triplicates, n=3; N.D.-not detectable). \*\* $P$ <0.005, \* $P$ <0.05. Representative cell images taken at the indicated time after infection, for stable (L, NDV), transient (M, SINV) and alternating (N, Adeno5 $\square$ E1A) SG formation are shown. Wild type HeLa cells were mock infected or infected for 4 or 12 h and fixed to examine localization of endogenous G3BP1 by immunostaining (O).

**FIG 3. EMCV infection results in the cleavage of G3BP1.** (A) Immunoblotting showing the kinetics of G3BP1 cleavage in EMCV-infected HeLa/G-G3BP1 cells. (B) HeLa stably expressing FLAG-G3BP1Q325E was infected with EMCV and G3BP1Q325E protein level was monitored by immunoblotting. (C) Western blot analysis of HeLa/G-G3BP1 cells

infected with EMCV. Lysates were prepared at the indicated time points after infection and subjected to immunoblotting by the indicated antibodies. (D) HeLa cells were transiently transfected with empty vector or expression vector for leader or 3C and analyzed for endogenous G3BP1 by Western blotting (left). HeLa/G-G3BP1 and HeLa/G-G3BP1Q325E were transiently transfected with empty vector or expression vector for leader or 3C and analyzed by Western blotting using anti GFP (right).

**FIG 4. HeLa/G-G3BPQ325E cells displayed stable formation of SG induced by EMCV infection.** Both HeLa/G-G3BP1 (A) and HeLa/G-G3BP1Q325E (B) cells were infected with EMCV. GFP fluorescence image of these cells at every 40 min is shown. (C) Quantitative analysis of SG formation pattern of HeLa/G-G3BP1Q325E cells infected with EMCV. (Error bars,  $\pm$ S.D. of triplicates,  $n=3$ ; N.D.-not detectable). \*\*  $P<0.005$ .

**FIG 5. Cleavage or knockdown of G3BP1 results in enhanced EMCV replication.** (A) HeLa/G-G3BP1 and HeLa/G-G3BP1Q325E cells were infected with EMCV. Total RNA was harvested at 12 h post infection and EMCV RNA was quantified by qPCR (upper). The culture supernatant was subjected to plaque titration (lower). (B) HeLa cells were either transfected with control siRNA or that targeted to G3BP1. After 48 h, G3BP1 was detected by Western blotting (upper left) or by staining using anti G3BP1 antibody (upper right). To investigate the effect of G3BP1 knockdown on viral replication, the cells were infected with EMCV for 12 h and total RNA was extracted and EMCV RNA was quantified by qPCR (bottom left). The culture supernatant was analyzed for viral titer (bottom right).

**FIG 6. Inhibition of G3BP1 in EMCV-infected cells results in sustained cytokine/chemokine mRNA accumulation.** HeLa/G-G3BP1 and HeLa/G-G3BP1Q325E cells were infected with EMCV. Culture supernatant was subjected to ELISA for IFN- $\beta$  (A). Total RNA was harvested at the indicated time points. mRNAs for (B) IFN- $\beta$ , (C) CXCL10, (D) IL-6 and (E) RANTES were determined by RT-qPCR. (F) Both HeLa/G-G3BP and HeLa/G-G3BPQ325E cells were infected with IAV $\square$ NS1 and IFN- $\beta$  mRNA was quantified as above (left). The lysate of IAV $\square$ NS1-infected HeLa/G-G3BP1 cells were examined for cleavage of G3BP1 by Western blotting (right). Data depicted are the representative of two independent experiments (Error bars,  $\pm$ S.D. of duplicates). \*\* $P$ <0.005, \* $P$ <0.05.

**FIG 7. IFN production and cytokine gene activation in HeLa/G-G3BP and HeLa/G-G3BPQ325E cells at early phase.** HeLa/G-G3BP1 and HeLa/G-G3BP1Q325E cells were mock-treated or infected with EMCV for indicated time. Total RNA was extracted and mRNA was quantified for IFN- $\beta$  (A), CXCL10 (B), IL-6 (C) and RANTES (D) by RT-qPCR.

**FIG 8. Knockdown of G3BP1 attenuates EMCV-induced cytokine/chemokine gene activation.** HeLa cells were either transfected with control siRNA or that targeted to G3BP1. After 48 h of incubation, cells were infected with EMCV for 12 h and total RNA was collected as indicated. mRNAs for (A) IFN- $\beta$ , (B) RANTES, (C) CXCL10 and (D) IL-6 were determined by RT-qPCR. Data are representative of two independent experiments. (Error bar,  $\pm$ S.D. of duplicates, N=2). \* $P$ <0.05.

**FIG 9. EMCV infection recruits MDA5 into SGs.** HeLa cells were mock-treated or infected with EMCV (MOI: 10) and fixed. The cells were stained for MDA5, G3BP1 and PI (A) or MDA5, TIAR and PI (B).

**FIG 10. Involvement of PKR in EMCV-induced SG and IFN- $\beta$  gene activation.** (A) Knockdown of PKR expression results in reduced SGs. HeLa cells transfected with siRNA targeting PKR for 48 h was examined for PKR expression by Western blotting (left). The cells were infected with EMCV for 6 h and stained for endogenous G3BP1 (middle). SG-containing cells were quantified (right). (B) HeLa cells infected with EMCV for 0, 4 and 12 h were analyzed for G3BP1, phospho-PKR, EMCV proteins and actin by immunoblotting. (C) HeLa cells transfected with siRNA targeting PKR for 48 h was mock treated or transfected with poly I:C or infected with IAV $\Delta$ NS1 or with EMCV. After 12 h, IFN mRNA was quantified by RT-qPCR  $^{**}P<0.005$ ,  $^{*}P<0.05$ .

**FIG 11. RIG-I was not cleaved after EMCV or PolioV infection.** (A) HeLa cells were either mock treated or infected with EMCV for indicated time. RIG-I was detected by Western blotting. (B) HeLa cells were mock treated or infected with Polio V for 9 h. G3BP1 (left) and RIG-I (right) were examined by Western blotting.

**FIG 12. EMCV 3C, but not leader inhibits SG.** (A) HeLa/G-G3BP1 and HeLa/G-G3BP1Q325E were transiently transfected with empty vector or expression vector for leader or 3C for 48 h. Cells were treated with 0.5 mM Sodium arsenite for 30min, fixed and stained for TIAR, a SG marker. (B) HeLa cells were transiently transfected with empty

633 vector or expression vector for leader or 3C (0 $\mu$ g, 2 $\mu$ g and 4 $\mu$ g) for 48 h. Cells were mock  
634 treated or transfected with long polyI:C (2 $\mu$ g/ $\mu$ L) for 12 h. Total RNA was collected and  
635 mRNA for IFN- $\beta$  was determined using RT-qPCR. Data are representative of three  
636 independent experiments. (Error bar,  $\pm$ S.D. of duplicates, N=3).

637

638



## Supplemental FIG S1.

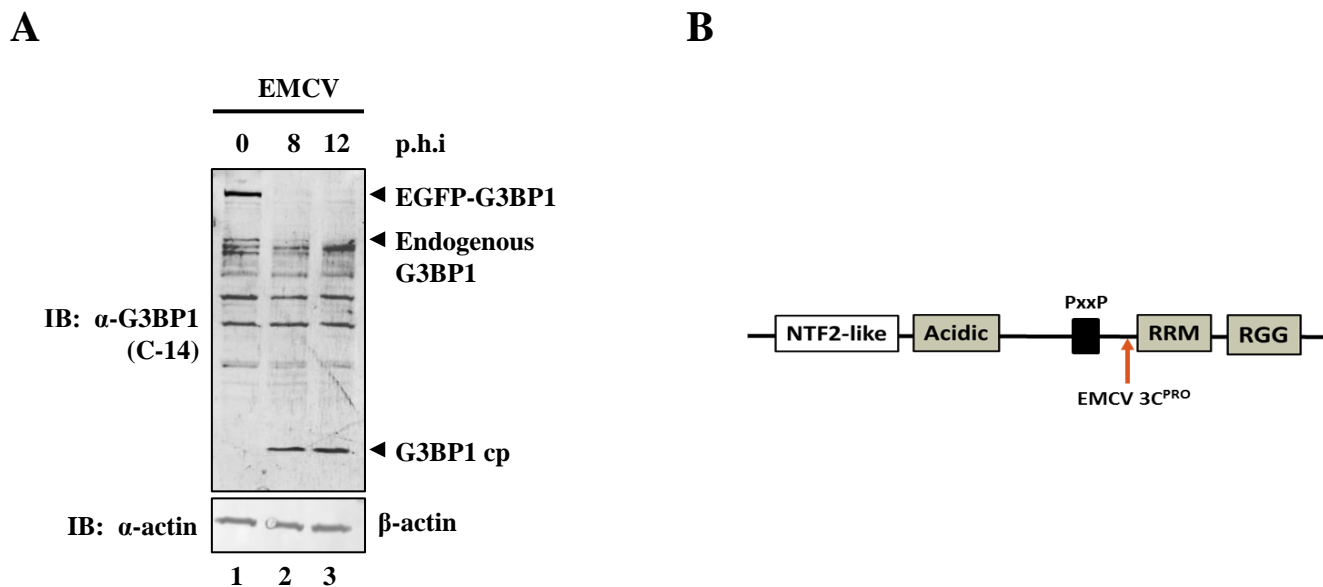


**FIG S1. Detection of C-terminal cleavage product of G3BP.** HeLa/G-G3BP1 cells were either mock treated or infected with EMCV. (A) Cell lysate was prepared at 0, 8, 12 h post infection and analyzed by Western blotting using antibodies against C-terminal region of G3BP1 or b-actin. (B) Cleavage site within the domain structures of G3BP1.

## Supplemental Movie Legends

**Movie S1. Real-time imaging of stress-granule marker, G3BP1 after NDV infection.** HeLa/G-G3BP cells were either mock-treated or infected with NDV. Live-cell imaging was initiated after 1 h post-infection with images captured every 10 min. Fluorescence images at indicated time after infection are shown.

**Movie S2. Real-time imaging of stress-granule marker, G3BP1 after IAV $\Delta$ NS1 infection.** HeLa/G-G3BP cells were either mock-treated or infected with IAV $\Delta$ NS1. Live-cell imaging was initiated after 1 h post-infection with images captured every 10 min. Fluorescence images at indicated time after infection are shown.

**Movie S3. Real-time imaging of stress-granule marker, G3BP1 after Adeno5WT infection.** HeLa/G-G3BP cells were either mock-treated or infected with Adeno5WT. Live-cell imaging was initiated after 1 h post-infection with images captured every 10 min. Fluorescence images at indicated time after infection are shown.

**Movie S4. Real-time imaging of stress-granule marker, G3BP1 after SINV infection.** HeLa/G-G3BP cells were either mock-treated or infected with SINV. Live-cell imaging was initiated after 1 h post-infection with images captured every 10 min. Fluorescence images at indicated time after infection are shown.

**Movie S5. Real-time imaging of stress-granule marker, G3BP1 after PolioV infection.** HeLa/G-G3BP cells were either mock-treated or infected with PolioV (MOI=1). Live-cell imaging was initiated after 1 h post-infection with images captured every 10 min. Fluorescence images at indicated time after infection are shown.

**Movie S6. Real-time imaging of stress-granule marker, G3BP1 after EMCV infection.** HeLa/G-G3BP cells were either mock-treated or infected with EMCV (MOI=10). Live-cell imaging was initiated after 1 h post-infection with images captured every 10 min. Fluorescence images at indicated time after infection are shown.

## Supplemental Movie Legends

### **Movie S7. Real-time imaging of stress-granule marker, G3BP1 after Adeno5ΔE1A infection.**

HeLa/G-G3BP cells were either mock-treated or infected with Adeno5ΔE1A. Live-cell imaging was initiated after 1 h post-infection with images captured every 10 min. Fluorescence images at indicated time after infection are shown.

### **Movie S8. Real-time imaging of stress-granule marker, G3BPQ325E mutant stable cells after EMCV infection.**

HeLa/G-G3BPQ325E cells were either mock-treated or infected with EMCV (MOI=10). Live-cell imaging was initiated after 1 h post-infection with images captured every 10 min. Fluorescence images at indicated time after infection are shown.

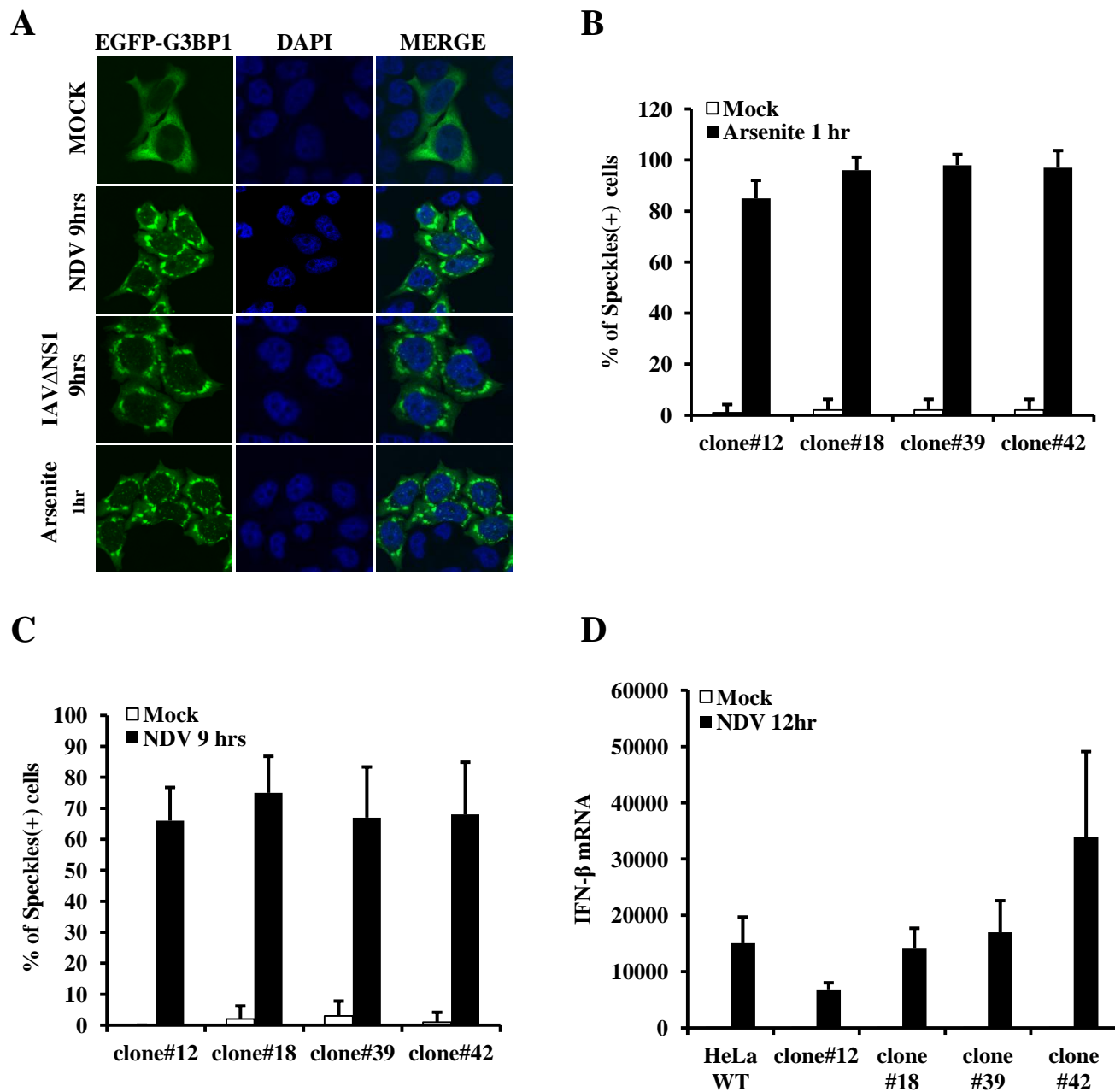
### **Movie S9. Real-time imaging of stress-granule marker, G3BP1 after TMEV infection.**

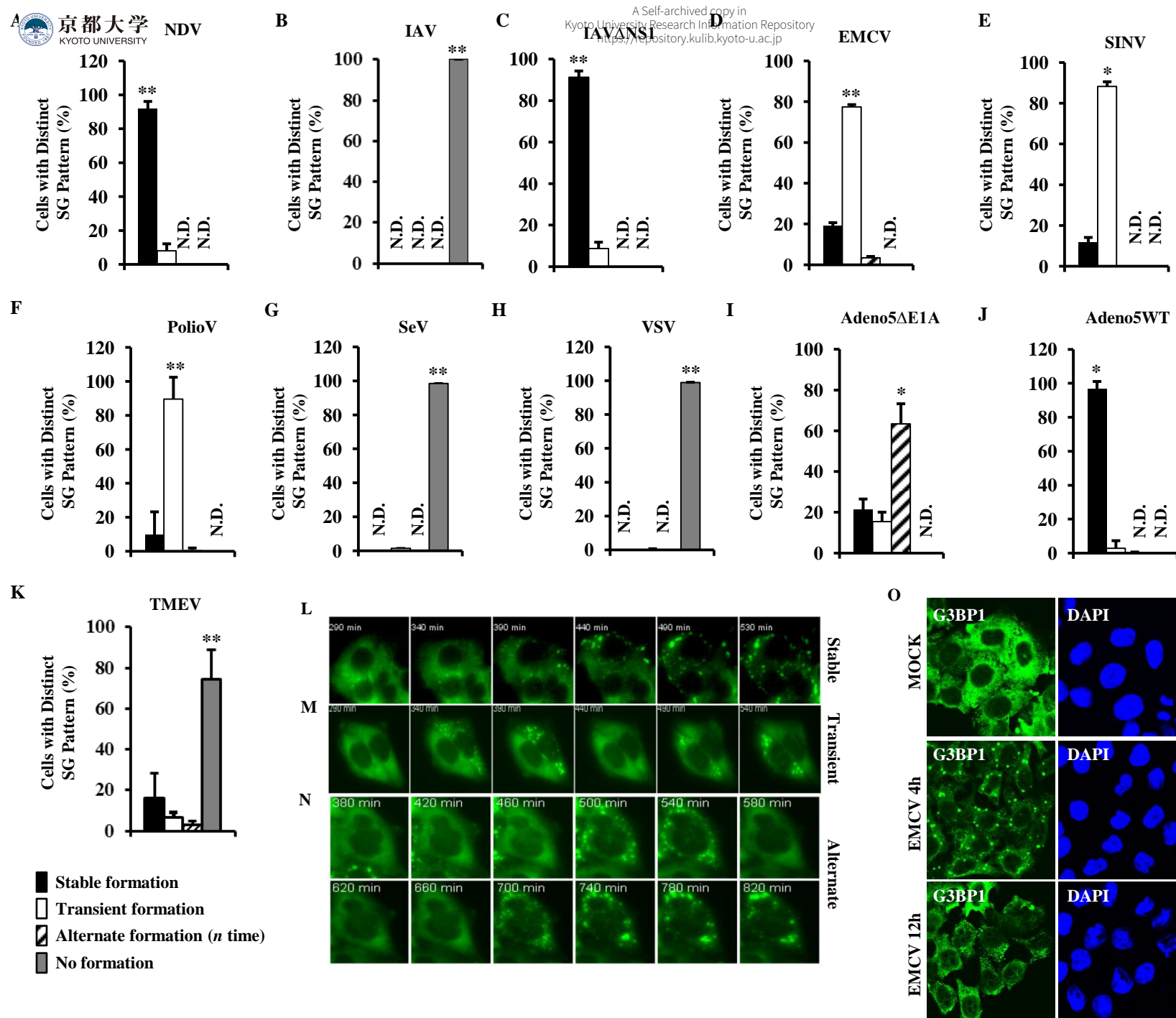
HeLa/G-G3BP cells were either mock-treated or infected with TMEV (MOI=10). Live-cell imaging was initiated after 1 h post-infection with images captured every 10 min. Fluorescence images at indicated time after infection are shown.

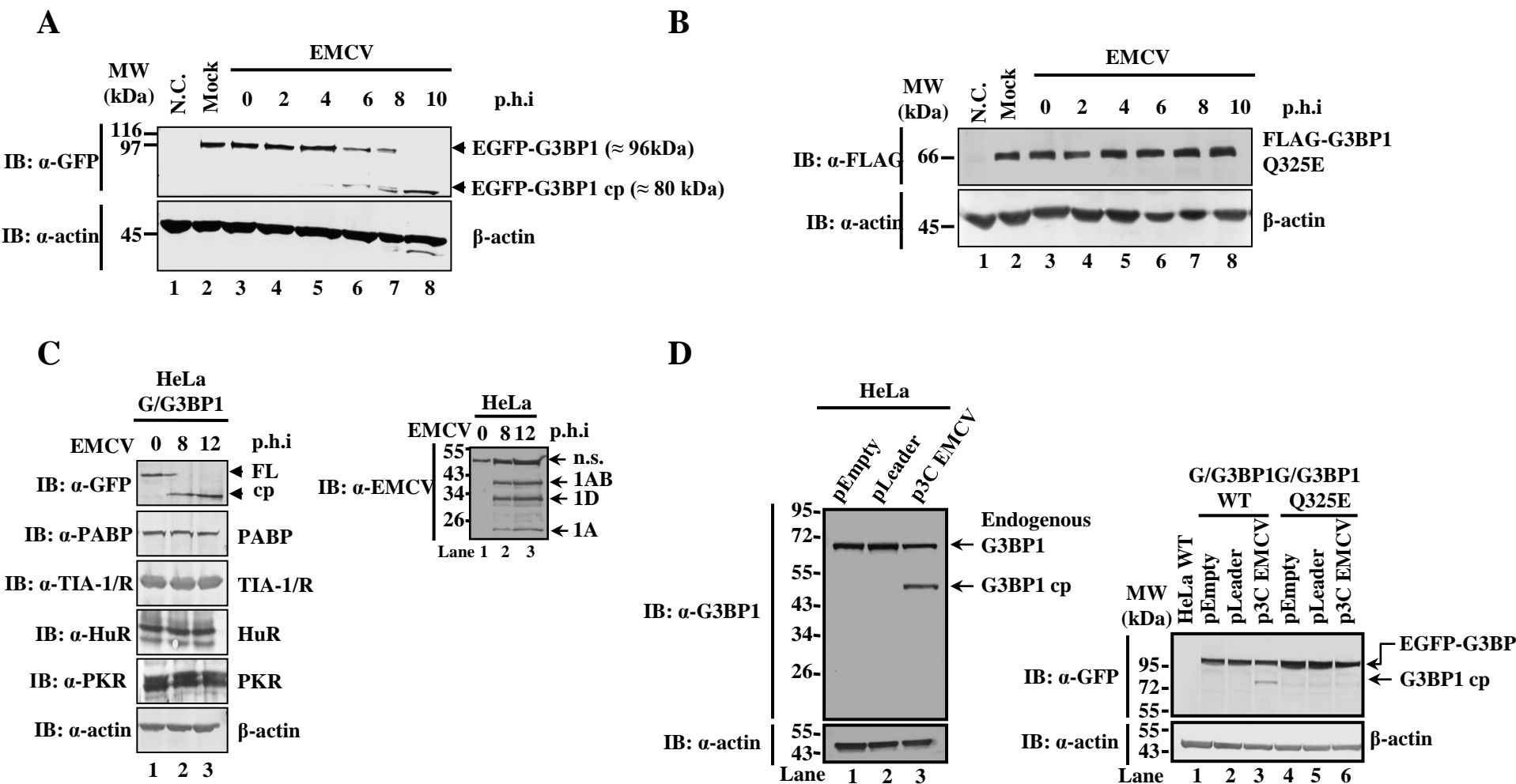
### **FIG S1. Detection of C-terminal cleavage product of G3BP.**

HeLa/G-G3BP1 cells were either mock treated or infected with EMCV. (A) Cell lysate was prepared at 0, 8, 12 h post infection and analyzed by Western blotting using antibodies against C-terminal region of G3BP1 or b-actin. (B) Cleavage site within the domain structures of G3BP1.

FIG. 1

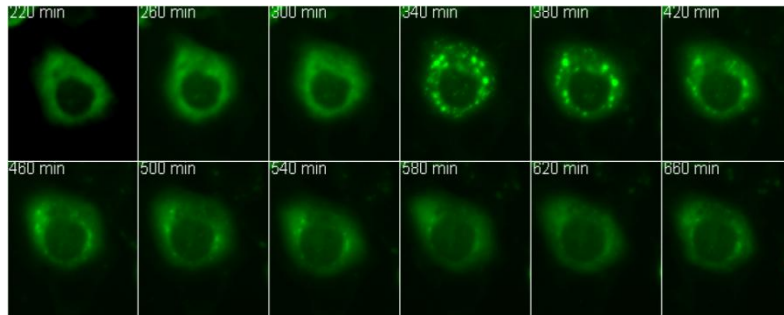






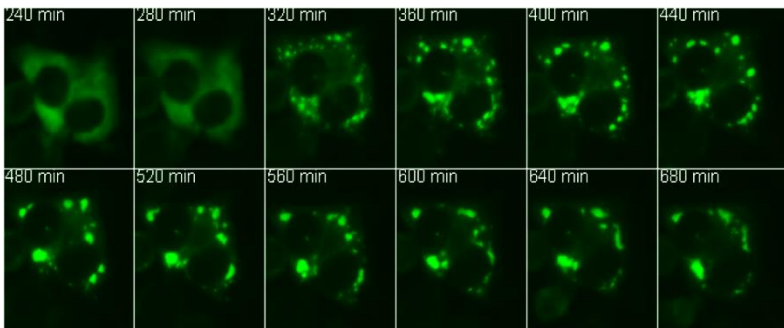
A

EGFP-G3BP1

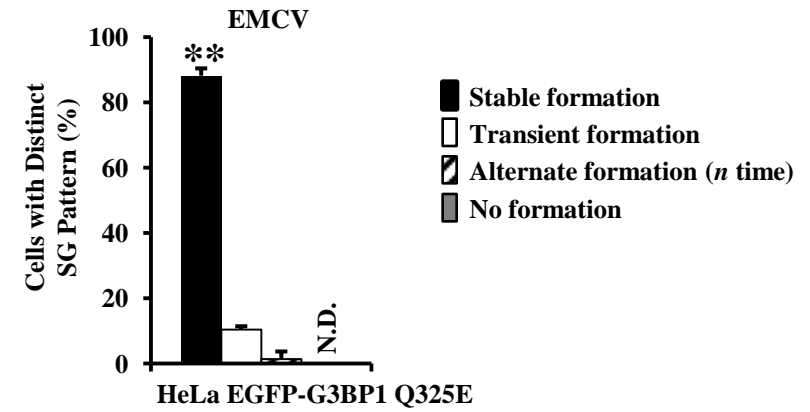


B

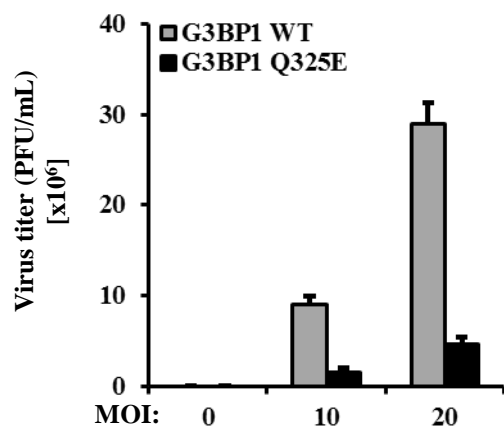
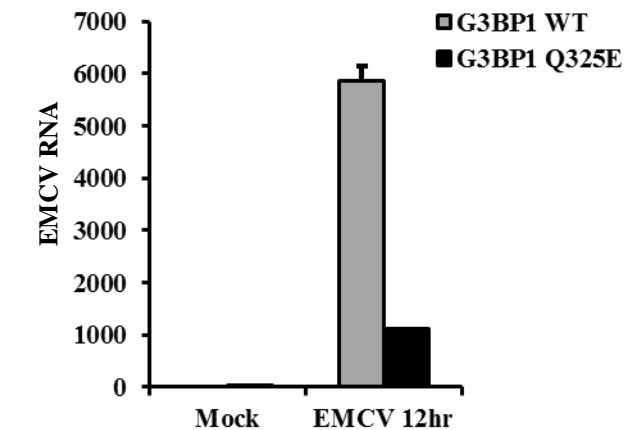
EGFP-G3BP1 Q325E



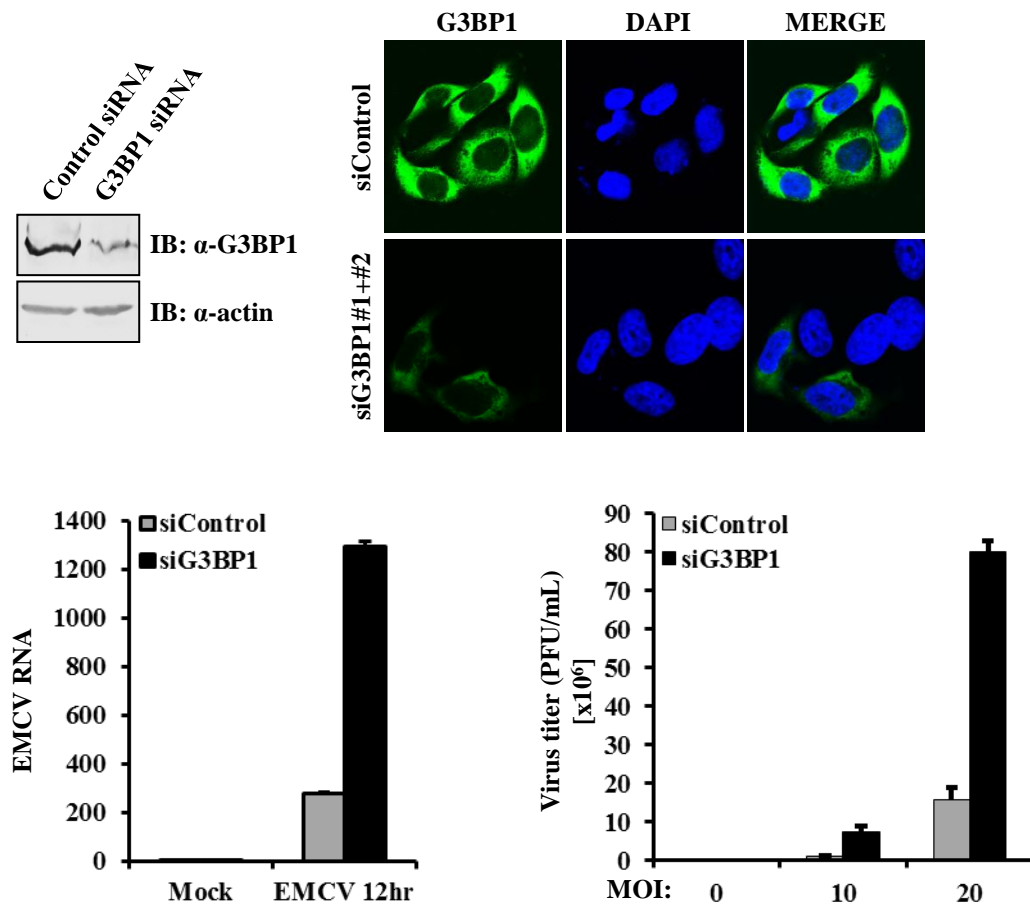
C



A

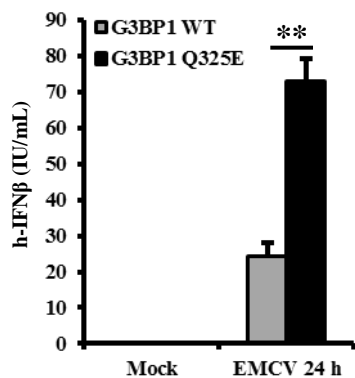


B

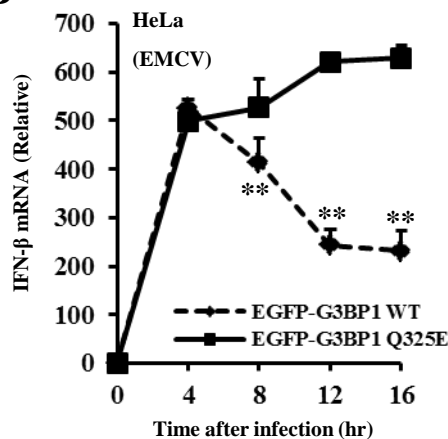




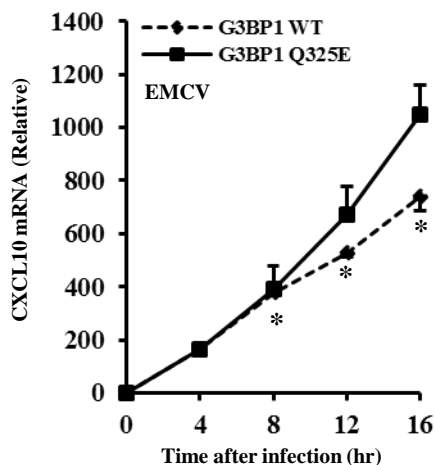
A



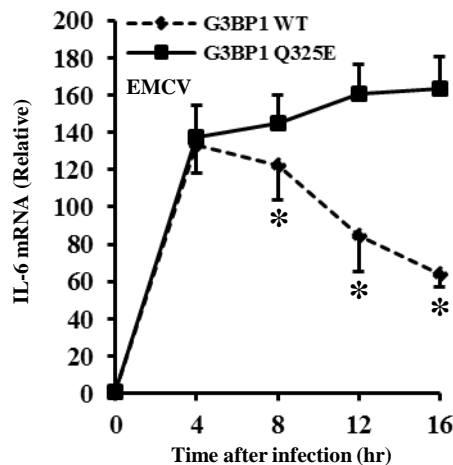
B



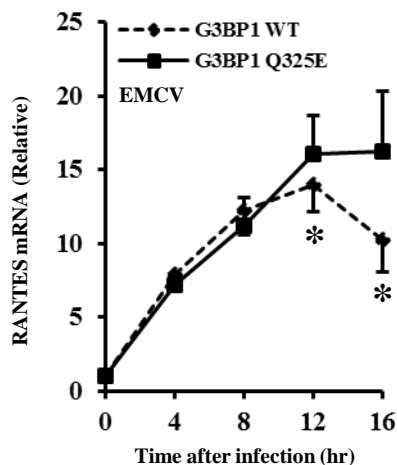
C



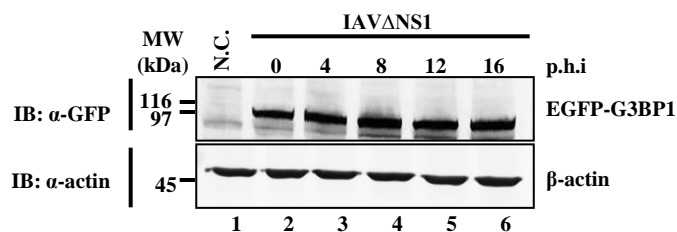
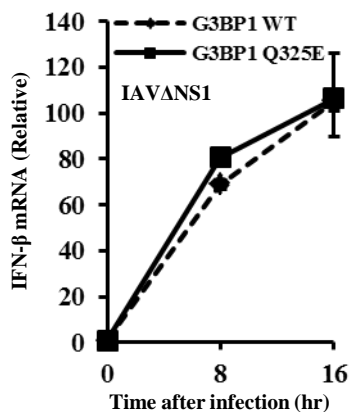
D



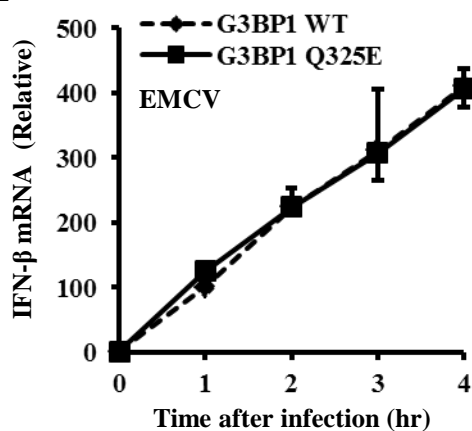
E



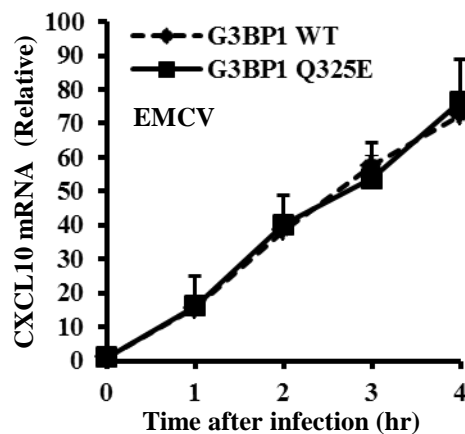
F



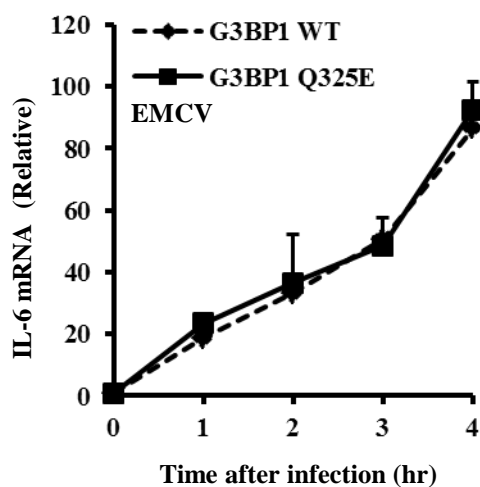
A



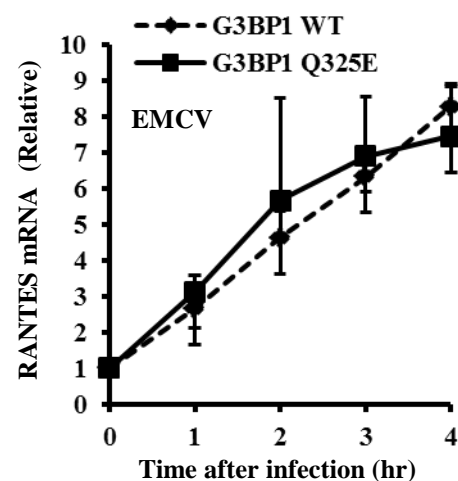
B

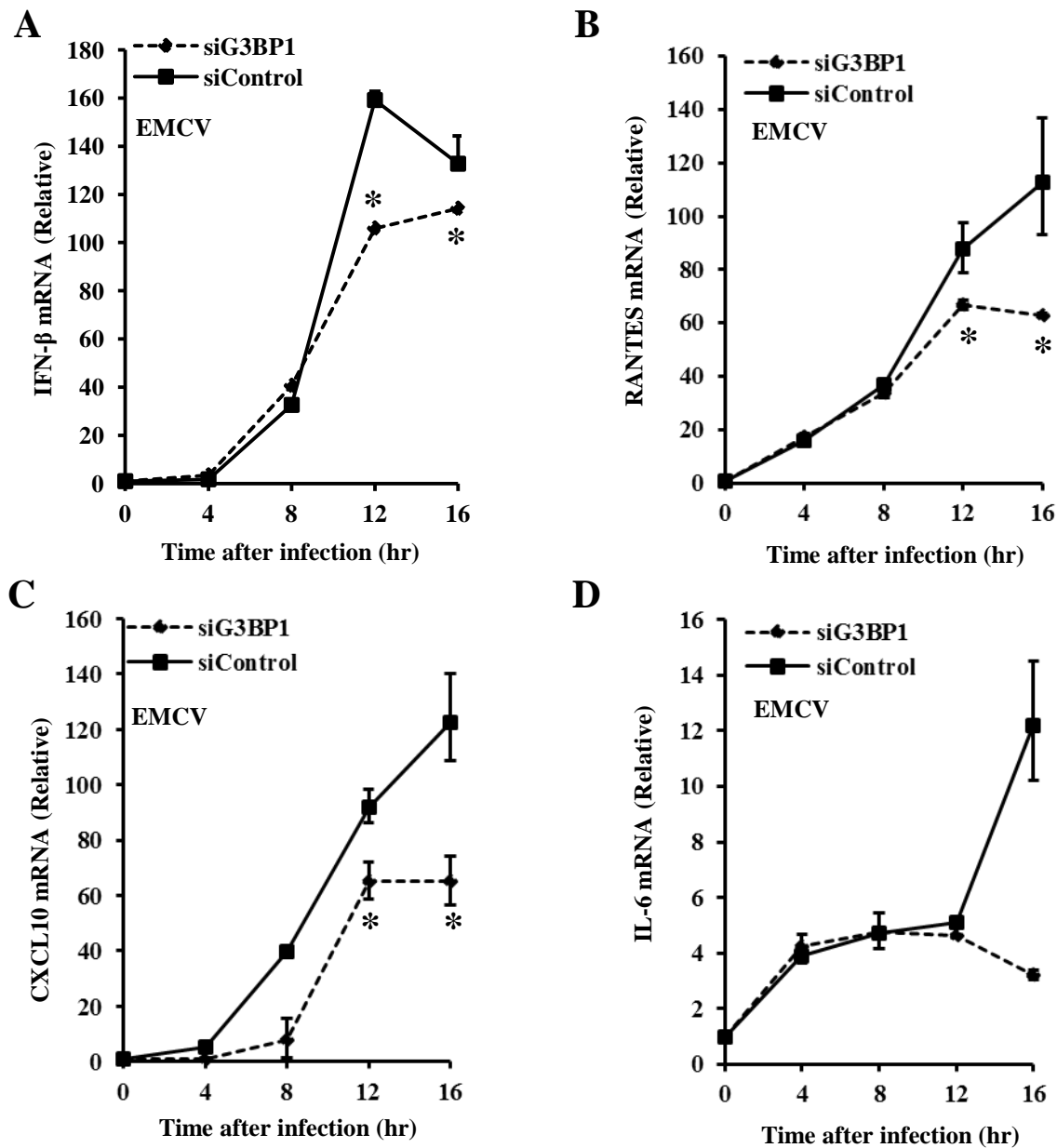


C

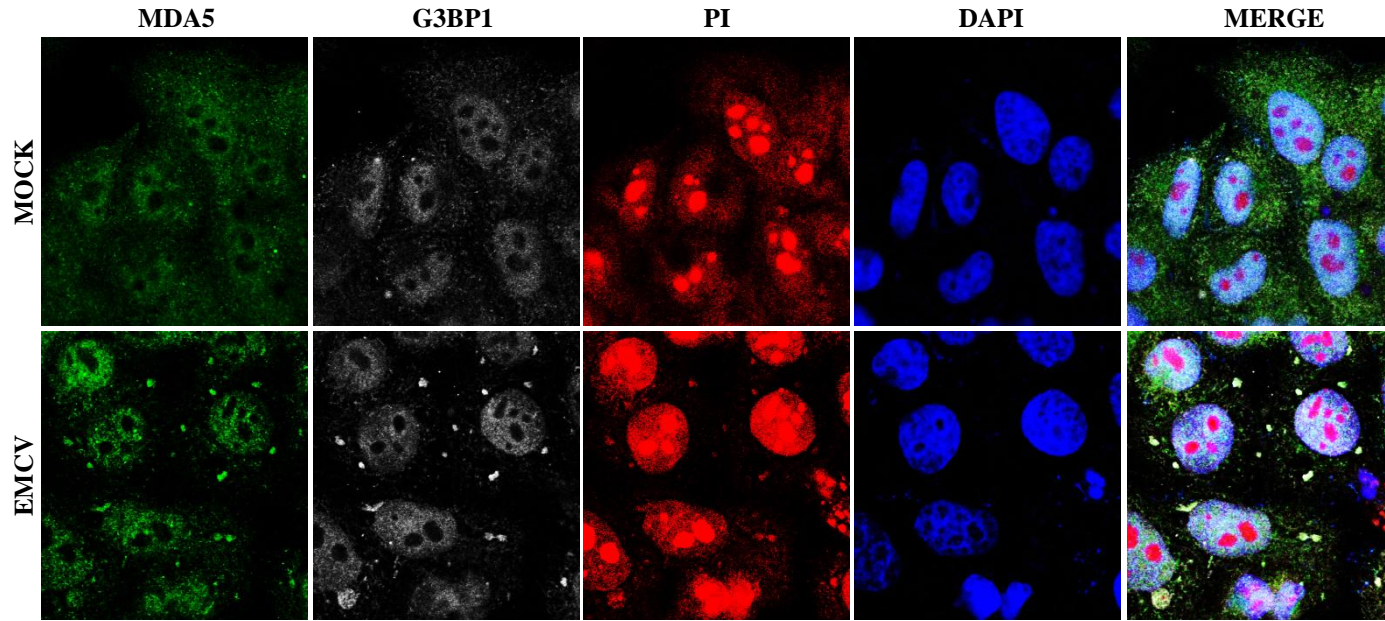


D

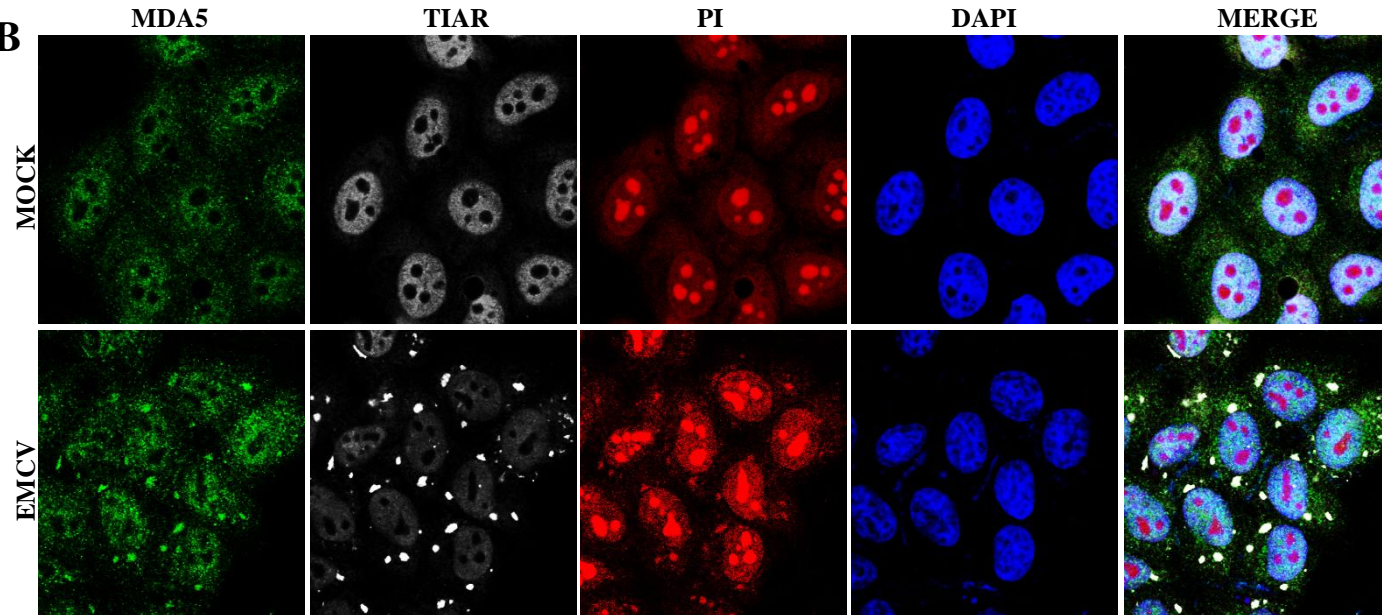




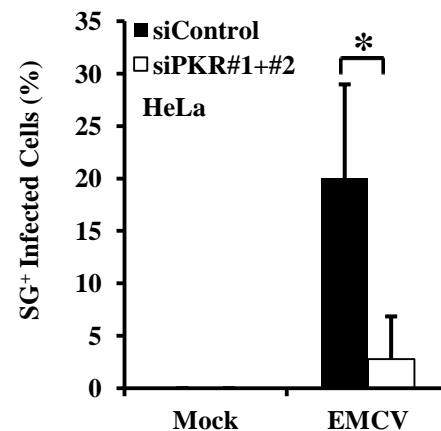
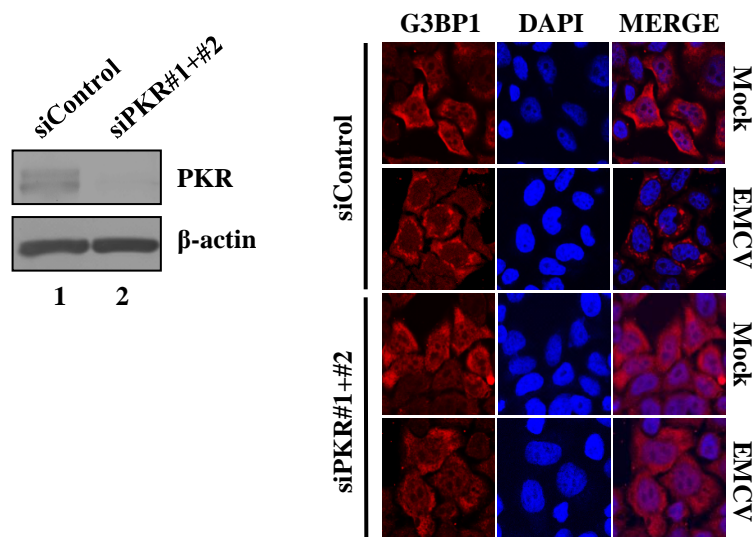
**A**



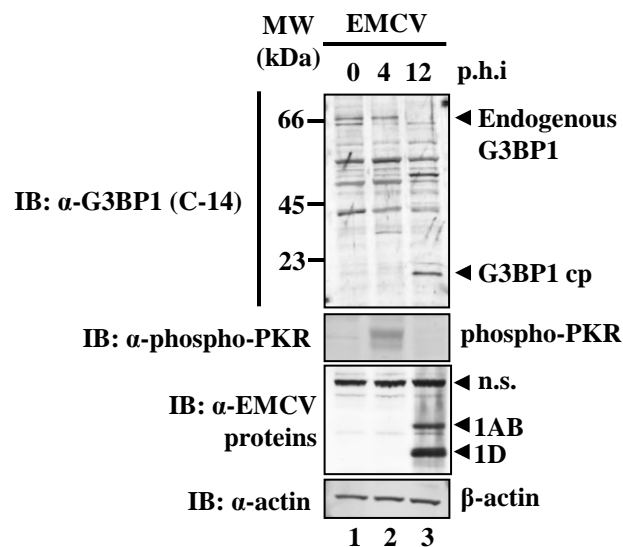
**B**



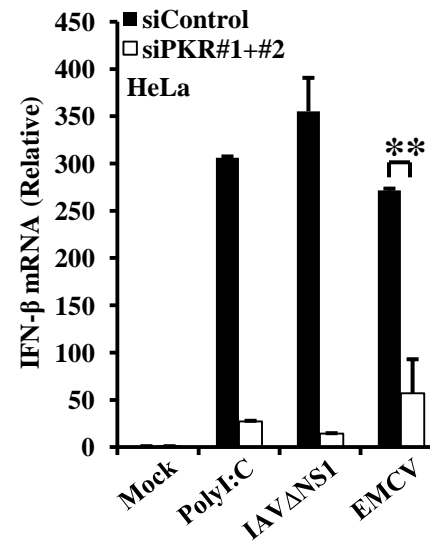
**A**



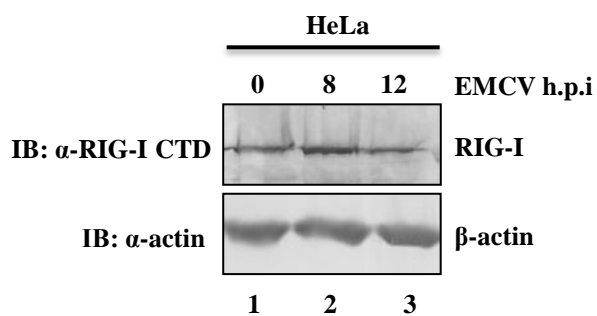
**B**



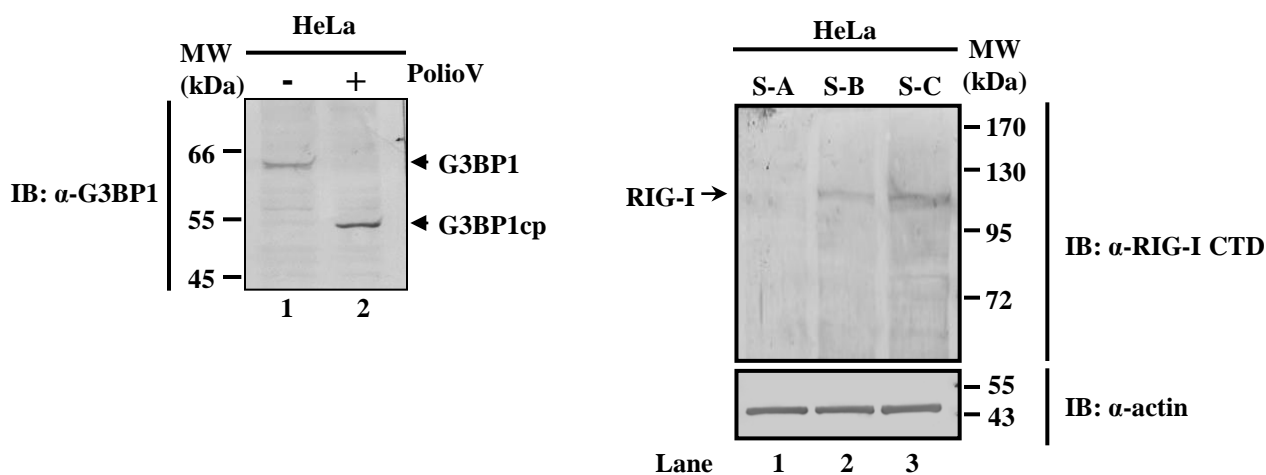
**C**



**A**



**B**



**Note:**

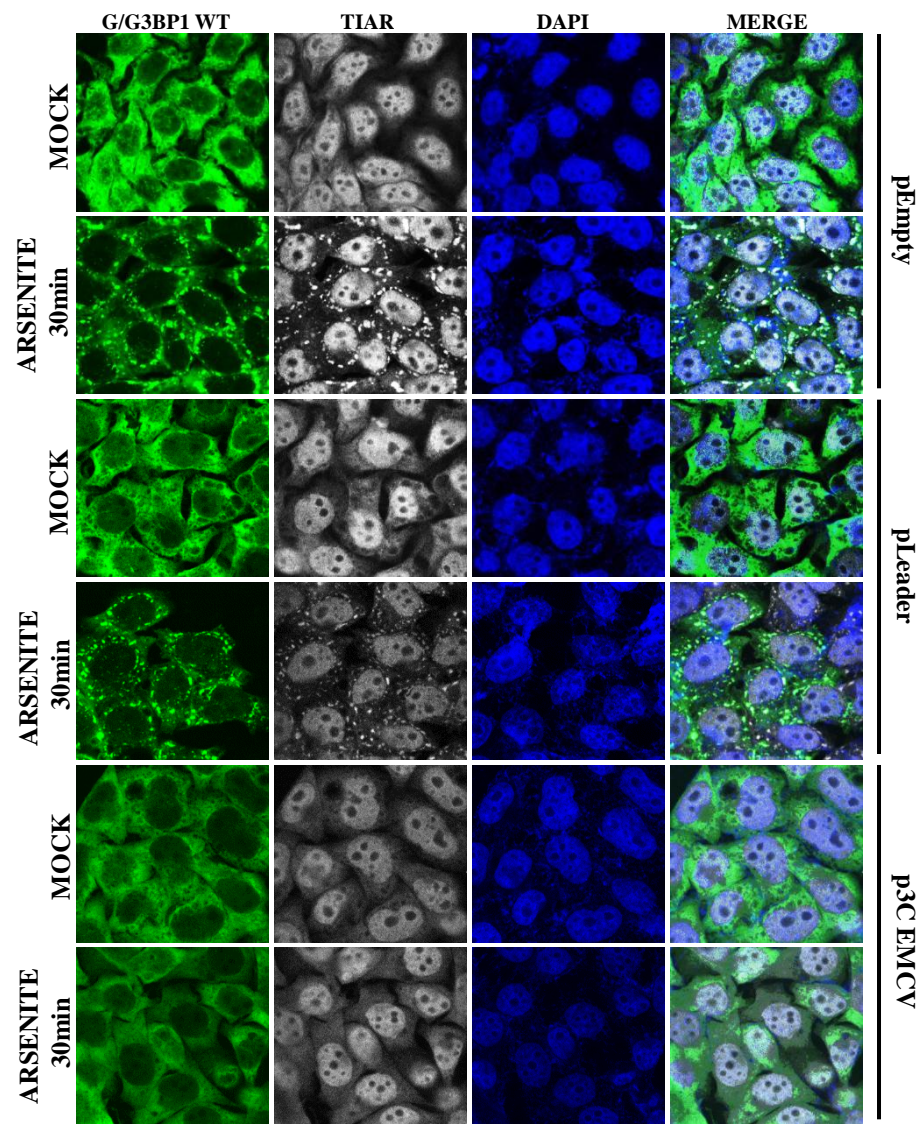
**S-A: Mock with shRIG-I**

**S-B: Mock infection**

**S-C: PolioV 9 h**



**A**



**B**

